α decay of Po and Rn isotopes using different choices of impinging frequency

Nitin Sharma* and Manoj K. Sharma
School of Physics and Materials Science, Thapar Institute of Engineering and Technology, Patiala 147004, Punjab, India

(Received 24 May 2022; accepted 11 August 2022; published 22 September 2022)

A comprehensive study of α particle emergence from $^{188–218}$Po isotopes is carried out within the framework of the preformed cluster model (PCM). The mass asymmetry coordinate and the interfragment separation play crucial roles in the identification of the most probable decay channel and the barrier penetration of decay fragments. First, the barrier characteristics are studied using two choices of radii [with surface diffuseness (C_i) and without surface diffuseness (R_i)]. The fragmentation behavior of ^{188}Po, ^{202}Po, and ^{218}Po isotopes is explored for the identification of the most probable decay channel in view of the structure of the fragmentation potential. The α decay is found to be the most prominent decay mode in the chosen set of isotopes. The preformation and penetrative probability of the decay fragments is studied with respect to increase in the neutron number of the parent nucleus. The α decay half-lives of polonium isotopes are calculated using classical assault frequency (ν_c) and quantum mechanical assault frequency (ν_q) and a comparison is made with the experimental data. Here, the term assault frequency is basically the impinging frequency of an α particle near the surface of the parent nucleus. Further, the α decay half-lives of the $^{198–220}$Rn isotopes are calculated using the effective assault frequency (ν_e) parameter, and a comparison is made with the available experimental data.

DOI: 10.1103/PhysRevC.106.034608

I. INTRODUCTION

The spontaneous emergence of the mass and energy from an unstable radioactive nucleus is termed radioactivity, which was given by Henry Becquerel in 1896 [1]. Generally, it is considered that a radioactive nucleus may try to reach a stable configuration via emergence of alpha (α) particle, beta (β) particle, and gamma (γ) decay modes. There are other radioactive decay modes such as cluster radioactivity (CR)[2,3], heavy particle radioactivity (HPR), spontaneous fission (SF) [4]. etc. It is observed that the α decay is the most common emission mode, and has higher decay probability among other competing modes (CR, HPR, SF, etc.). Further, α decay also works as a decisive factor for the stability analysis of nuclei belonging to heavy and superheavy mass regions [4–13]. Few experimental attempts [14] explore the continuous emission of α particles near $Z = 50$. α decay chains are also observed in the superheavy mass region, where successive α emission happens and the process terminates with spontaneous fission. Hence, the α decay plays important role in exploring the decay dynamics and the associated stability aspects.

Numerous experimental and theoretical attempts [10,13,15–26] were performed to understand the radioactive emergence of the α particle. Several nuclear models such as the generalized liquid drop model (GLDM) [27,28], the cluster formation model (CFM) [29], double folding potential model [30], the unified fission model (UFM) [31], the analytical superasymmetric fission model (ASAFM), [32] and the preformed cluster model (PCM) [33,34] were introduced to understand the cluster-core interplay within the radioactive parent nuclei. The above mentioned models are based on some assumptions and are worked out in terms of certain coordinates to study different decay properties associated with unstable nuclei. In the generalized liquid drop model (GLDM), the macroscopic liquid drop energies play a key role to give different decay channel properties. On the other hand, in the unified fission model (UFM) the preformation or spectroscopic factors are taken to be unity and the decay half-lives are calculated using the barrier characteristics. Similarly, the preformed cluster model (PCM) [35] has successfully explored different ground state decay mechanisms such as α decay, CR, HPR, SF [36,37], etc. In this model, a cluster is supposed to be in a preborn state within the parent nucleus and the cluster core interplay is explored using the mass asymmetry coordinates and the relative separation distances. These coordinates are further employed collectively and give the preformation probability of the decaying fragments, which in turn serves as an important tool for the estimation of the decay half-life, the decay constant, etc. The stability analysis of a radioactive nucleus depends on the decay constant, which is a product of preformation probability (P_0), penetration probability, and the barrier assault frequency. The term "impinging frequency" or "assault frequency" is the frequency of the α particle near the surface of the parent nucleus. The preformation probability is calculated using the stationary Schrödinger equation in terms of the mass asymmetry coordinate and the penetration probability is calculated via the Wentzel-Kramers-Brillouin (WKB) approximation method. In the present work the role of assault frequency (ν_0) is calculated using classical and quantum mechanical views. In the classical view, the assault

*nitinsharma2295@gmail.com

frequency is calculated using the decay energy or the total kinetic energy, which is assumed to be shared among the decay fragments [38]. In the quantum mechanical view, the cluster is supposed to vibrate near the surface of the parent nucleus under the influence of a harmonic oscillator potential [39]. Furthermore, some attempts were made [40,41] in which modified assault frequency parameters were introduced. It is assumed that the preformation factors are included in such calculations. In the present paper, an attempt is made to explore the role of effective assault frequency parameters in terms of the Q value of the decay channel.

As discussed earlier, the α particle emission is one of the major common emission modes in a radioactive nucleus which may attain a stable configuration under the influence of proton or neutron shell closure effects. It will be of interest to study such effects for a chosen set of nuclear isotopes. In this paper, α decay analysis of $^{188-218}$Po isotopes is performed, which after α decay gives the lead (Pb) isotopes as daughter fragments. The calculations are performed using PCM, and the primary goals of the work are (i) to study the behavior of the preformation probability, penetration probability, and assault frequency with respect to the neutron number of the parent or daughter nucleus; (ii) to make a comparative analysis of α decay half-lives using different choices of assault frequency; and (iii) to explore the relevance of the effective assault frequency parameter, which may further help exploration of the α decay properties. The overview of this paper is as follows. Section II gives a brief description of the preformed cluster model (PCM). In Sec. III, α decay analysis of Po isotopes is carried out using different assault frequencies. The effective frequency parameter is given, and further this parameter is used to calculated the decay half-lives of Rn isotopes. Finally, a summary of the observations and conclusions drawn is outlined in Sec. IV.

II. PREFORMED CLUSTER MODEL (PCM)

In the present paper, the calculations are performed using the preformed cluster model (PCM). PCM is based on the quantum mechanical fragmentation theory (QMFT) [52–54]. The main assumption of the model is that the cluster is in a preformed state within the parent nucleus, as follows the collective clusterization approach, which treats all probable decay modes such as α decay, CR, HPR and spontaneous fission on parallel footing. The methodology mainly works out in terms of the mass (or charge) asymmetry coordinate η and R coordinates. The stability analysis of a nucleus is estimated by calculating the decay half-life $T_{1/2}$ and decay constant λ, which can be obtained as

$$T_{1/2} = \frac{\ln 2}{\lambda}, \quad \lambda = \nu P_0 P. \tag{1}$$

Here, ν and P_0 are the barrier assault frequency and preformation probability respectively, and P refers to the penetration probability (R motion). The assault frequency can be calculated via different methods or sometimes taken as constant (nearly 10^{21}). In the present work two type of assault frequencies, i.e., classical assault frequency (ν_c) and quantum assault frequency (ν_q), are explored. In the classical view, the assault

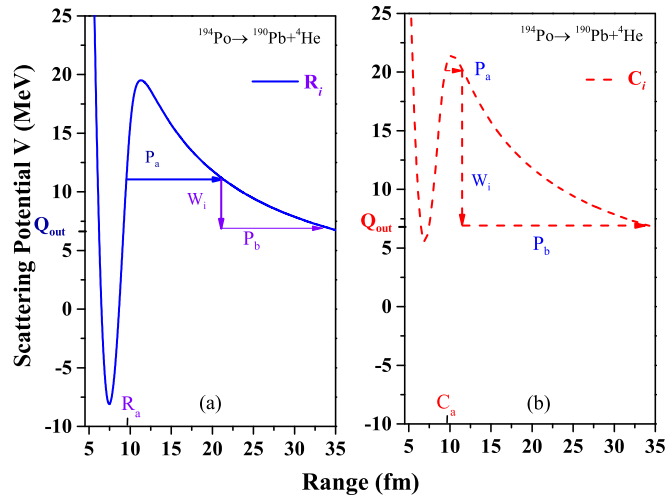

FIG. 1. The scattering potential $V(R)$ for the α decay using (a) effective sharp radius R_i (without surface diffuseness) and (b) Süssmann central radii C_i (with surface diffuseness).

frequency ν_c is calculated as

$$\nu_c = \frac{(2E_2/\mu)^{1/2}}{R_0}, \tag{2}$$

where R_0 is the radius of the parent nucleus, μ is the reduced mass, and E_2 is the kinetic energy of the emitted cluster. Since the emitted cluster and the daughter nucleus are produced in the ground state, the entire positive Q value of the decay is the total kinetic energy ($Q = E_1 + E_1$) available for the decay process, which is shared between the two fragments, such that the energy of the emitted cluster is (1 and 2 stand, respectively, for daughter and cluster)

$$E_2 = \frac{A_1}{A} Q, \tag{3}$$

and E_1 is the recoil energy of the daughter nucleus. In quantum picture, the cluster is assumed to be vibrating in a harmonic oscillator potential near the surface of the parent nucleus [39]. The quantum assault frequency (ν_q) is given as

$$\nu_q = \frac{\left(G + \frac{3}{2}\right)\hbar}{1.2\pi\mu R^2}. \tag{4}$$

G denotes the global quantum number of a cluster state and is given using the Wildermuth rule [55]:

$$G = 2n + l = \sum_{i=1}^{4} g_i. \tag{5}$$

The value of g_i is given as 4 for $(N, Z) \leqslant 82$, 5 for $82 < (N, Z) \leqslant 126$, and 6 for $(N, Z) > 126$, where N, Z are the neutron and proton numbers of the parent nucleus. For further details see Ref. [39,56,57]. The fragmentation potential V reads as

$$V_R(\eta) = -\sum_{i=1}^{2} B(A_i, Z_i) + V_C(R, Z_i, \beta_{\lambda i}, \theta_i) + V_P(R, A_i, \beta_{\lambda i}, \theta_i). \tag{6}$$

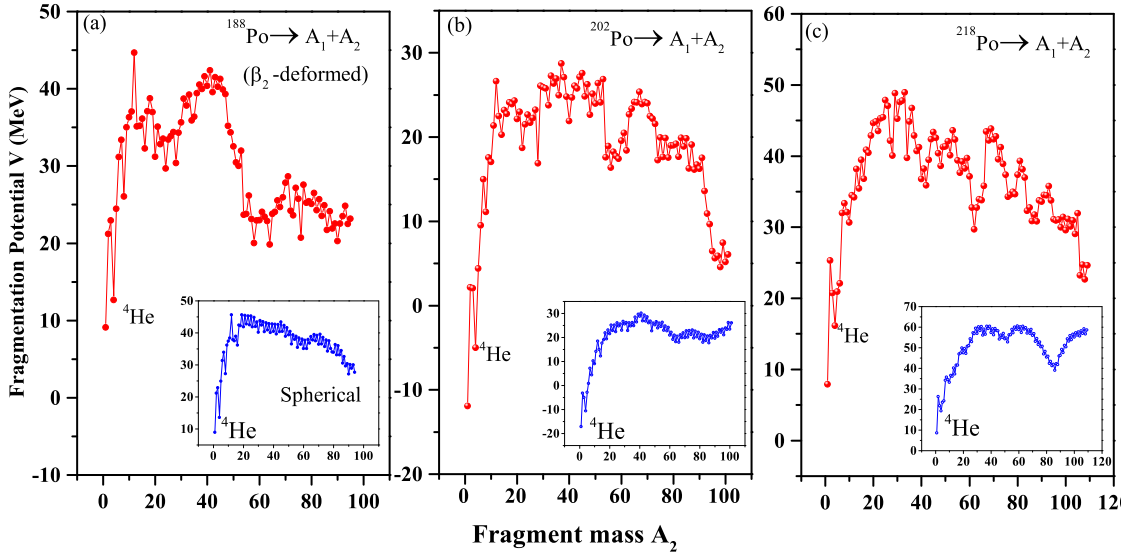

FIG. 2. The fragmentation potential V as a function of fragment mass A_2 for (a) ^{188}Po, (b) ^{202}Po, and (c) ^{218}Po isotopes using deformed and spherical (inset) choices of the decaying fragments.

Here B_i represents the ground state binding energies taken from [58]. The quadrupole deformation (β_2) values are taken from [59]. V_c denotes the Coulomb potential and V_p is the nuclear proximity potential, written as

$$V_{Pij}(s) = 4\pi\overline{R}\gamma b\Phi(s), \tag{7}$$

where s is the surface separation of fragments, $\gamma = 0.9517[1 - 1.7826(N - Z/A)^2]$ MeV fm^{-2} (the surface energy constant), and $b = 0.99$ is the nuclear surface thickness. $\overline{R}$ is the mean curvature radius and Φ is the universal function;

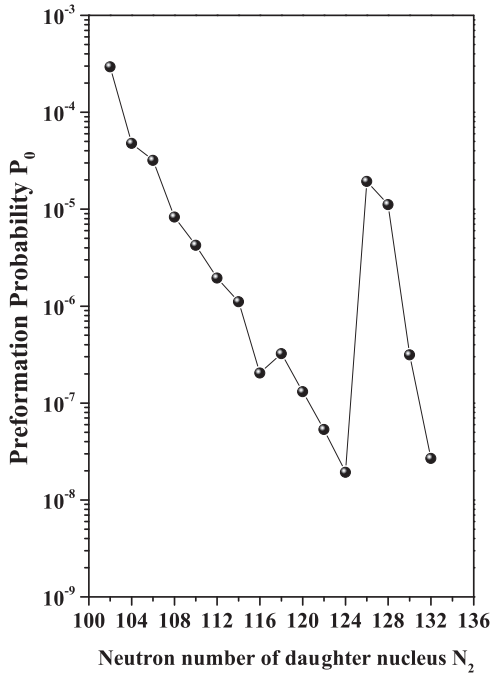

FIG. 3. The preformation probability P_0 as a function of neutron number N_2 for $^{188-218}$Po isotopes.

for more details, see Refs. [60,61]. The calculated fragmentation potential V is further used to calculate the preformation probability by solving the Schrödinger equation in the η coordinate at fixed $R = R_a$,

$$\left\{-\frac{\hbar^2}{2\sqrt{B_{\eta\eta}}}\frac{\partial}{\partial\eta}\frac{1}{\sqrt{B_{\eta\eta}}}\frac{\partial}{\partial\eta} + V_R(\eta)\right\}\psi^{\nu}(\eta) = E^{\nu}\psi^{\nu}(\eta), \tag{8}$$

with $\nu = 0, 1, 2, 3, \ldots$ referring to ground state ($\nu = 0$) and excited state ($\nu \neq 0$) solutions. The penetration probability of P of the emitted fragments is obtained using the Wentzel-Kramers-Brillouin (WKB) integral, and determined by following expression:

$$P = P_a W_i P_b. \tag{9}$$

Here, the transmission probability consists of three contributions, as shown in Fig. 1:

(i) the penetrability P_a from R_a to R_i,

$$P_a = \exp\left[-\frac{2}{\hbar}\int_{R_a}^{R_i}\{2\mu[V(R) - V(R_i)]\}^{1/2}dR\right], \tag{10}$$

(ii) the inner deexcitation probability W_i at R_i,

$$W_i = \exp(-bE_i); \tag{11}$$

(iii) the penetrability P_b from R_i to R_b,

$$P_b = \exp\left[-\frac{2}{\hbar}\int_{R_i}^{R_b}\{2\mu[V(R) - Q]\}^{1/2}dR\right]. \tag{12}$$

This indicates that the penetration process begins at $R = R_a$ and terminates at $R = R_b$ with $V(R_b) = Q$ value. The concept of de-excitation probability W_i is taken unity from the excitation model of Greiner *et al* [62]. The first turning point (R_a) of the

penetration path is defined as

$$R_a = R_1(\alpha_1) + R_2(\alpha_2) + \Delta R$$
$$= R_t(\alpha) + \Delta R \tag{13}$$

with radius vectors R_i ($i = 1, 2$),

$$R_i(\alpha_i) = R_{0i}\left[1 + \sum_{\lambda} \beta_{\lambda i} Y_{\lambda}^{(0)}(\alpha_i)\right], \tag{14}$$

where

$$R_{0i} = \left[1.28A_i^{\frac{1}{3}} - 0.76 + 0.8A_i\right] \text{fm}. \tag{15}$$

α_i is the angle between the symmetry axis and the radius vector of the colliding nucleus, and ΔR is the only parameter of the model (known as neck-length parameter), which assimilates the neck formation effects. Further, the surface diffuseness effects can enter through the Süssmann central radii C_i [63] as

$$C_i = R_i\left(1 - b^2/R_i^2 + \cdots\right), \tag{16}$$

where b is the diffuseness parameter.

III. CALCULATIONS AND DISCUSSIONS

This section represents the theoretical analysis of α emission from $^{188–218}$Po isotopes using preformed cluster model. The calculations are done using quadrupole deformation (β_2) with cold-elongated configuration. First, in section III A, the fragmentation analysis of Po isotopes is carried out using the fragmentation potential. The importance of neutron shell closure effects is explored using the preformation probability and the penetration probability. The decay half-lives of the polonium isotopes is calculated using two choices of assault frequencies (ν_c and ν_q). In sec.III B, the effective assault frequency of the polonium isotopes is calculated and an effort is made to estimate $T_1/2$ using a Q-value dependent assault frequency parameter. Further, in Sec. III C, the α decay half-lives of Rn isotopes are calculated using the effective assault-frequency parameter ν_e given in sec.III B.

A. α decay analysis of $^{188–218}$Po isotopes using different assault frequencies

In this section, isotopic analysis of Po nuclei is carried out using the preformation probability (P_0), penetration probability (P), and the assault frequency (ν). The explored data of P_0, P, and ν are used to estimate the half-lives of the Po isotopes. The decay half-lives are also affected by the surface diffuseness of the decaying fragments. It is suggested by different authors [64,65] that the surface diffuseness along with the deformation effects play important roles in the decay mechanism. Similarly, in [66] it is concluded that nuclear surface diffuseness is an important property that must be added along with the deformation effects for lighter clusters ($A_2 < 20$). As we are interested in α particle emission in this work, as a first step a comparison of barrier characteristics without surface diffuseness (R_i) and with surface diffuseness (C_i) is made and shown in Fig. 1. Here, we are interested in studying the interfragment radii with inclusion of surface diffuseness (C_i) or without surface diffuseness (R_i). The difference in the barrier characteristics is due to the change in the proximity potential and the Coulomb potential. The barrier position and the barrier height are different for both cases. Hence, the penetration probability for both cases gets modified accordingly. We performed calculations using both radii, and C_i gives better agreement with experimental data (this will be discussed in detail in Fig. 6).

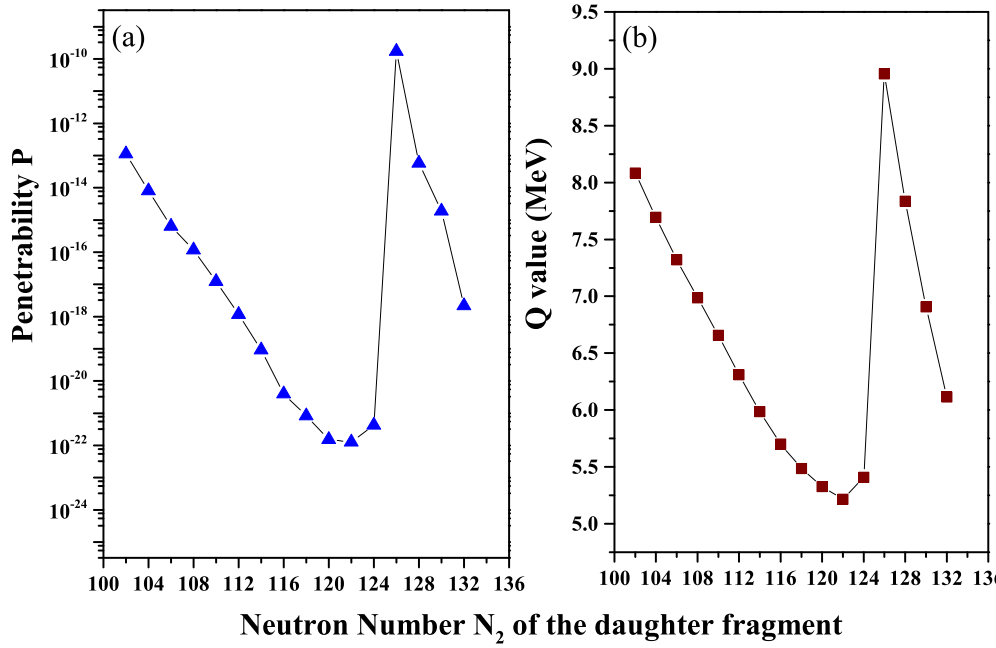

FIG. 4. The PCM calculated (a) penetration probability P and (b) the Q value of the α decay channel as a function of neutron number of the daughter fragment N_2.

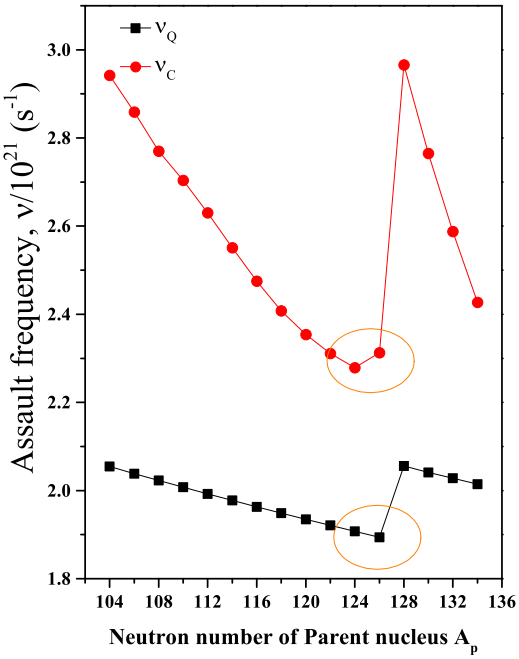

FIG. 5. Calculated (a) quantum assault frequency (ν_q) and (b) classical assault frequency (ν_c) as a function of neutron number of the parent nucleus.

After the analysis of surface diffusion effects, the fragmentation potential $V_R(\eta)$ is calculated, which will further help us to choose the most probable decaying fragments of the exit channel. The fragmentation potential for ^{188}Po, ^{202}Po, and ^{218}Po isotopes as a function of fragment mass A_2 is shown in Figs. 2(a)–2(c). The fragmentation structure for spherical choice of the decaying fragment is also shown within the insets. The minima in the fragmentation potential represent the most probable decay fragment along with its complementary fragment for both spherical and deformed choices. One can observe from the figure that $A_2 = {}^4$He is located at minima for all three isotopes and may be treated as one of the most probable fragments along with its complementary fragment. It may be concluded that, independent of deformation effects, the α decay is the most prominent decay choice among its competing decay channels for the chosen isotopes of polonium. Furthermore, one can observe that the fission region changes from symmetric to asymmetric mode when one goes from ^{188}Po to ^{218}Po isotope for the spherical choice of the decaying fragment. For the deformed choice, the fission region changes from asymmetric to nearly symmetric mode. It is relevant to note that α decay is observed experimentally for this nucleus; other decay modes such as CR or SF are not yet observed. Hence, in the present work we are interested in studying the α particle emission only. Further, the preformation probability P_0 is calculated by solving the stationary Schrodinger equation in terms of the η coordinate. In Fig. 3, preformation probability is plotted with respect to neutron number N_2 of the daughter fragment. It is observed that P_0 decreases with increase in the neutron number up to $N_2 = 124$ (for parent nucleus $N = 126$) and increases abruptly with addition of two more neutrons in the parent nucleus. Such behavior of P_0 is due to influence of neutron shell effects ($N = 126$), and one may conclude that the α cluster preformation probability decreases as the nucleus approaches the shell closure. The P_0 value is found to be maximum at $N_2 = 126$ (with $N = 128$) because the preformation probability is higher for the case where the α particle is accompanied by a stable nucleus complementary fragment. Hence, preformation factors strongly depend on the shell effects effects of the parent nucleus as well as those of the decaying fragments.

After the analysis of P_0, the penetration probability P is calculated using the WKB approximation. Figure 4(a) represents

TABLE I. PCM calculated preformation probability (P_0), penetrability (P), and the assault frequency (ν_c) for the α decay of $^{188-218}$Po isotopes and a comparison of these values is made with theoretical models SAM and GLDM [42,43] calculated values.

Parent	PCM				SAM [42]				GLDM [43]			
nucleus	$\log_{10} P_0$	$\log_{10} P$	$\log_{10} P_0 P$	$\nu/10^{21}$ (s^{-1})	$\log_{10} P_0$	$\log_{10} P$	$\log_{10} P_0 P$	$\nu/10^{21}$ (s^{-1})	$\log_{10} P_0$	$\log_{10} P$	$\log_{10} P_0 P$	$\nu/10^{21}$ (s^{-1})
^{188}Po	−3.531	−12.950	−16.482	2.942					−1.832	−16.089	−17.922	1.452
^{190}Po	−4.319	−14.091	−18.410	2.859	−1.348	−17.17	−18.518	1.41	−1.477	−17.228	−18.706	1.411
^{192}Po	−4.496	−15.197	−19.694	2.771	−1.336	−18.34	−19.676	1.37	−1.350	−18.407	−19.758	1.371
^{194}Po	−5.080	−15.925	−21.006	2.704	−1.325	−19.47	−20.795	1.33	−1.387	−19.488	−20.875	1.335
^{196}Po	−5.370	−16.913	−22.284	2.630	−1.312	−20.69	−22.002	1.30	−1.341	−20.690	−22.032	1.299
^{198}Po	−5.710	−17.936	−23.646	2.551	−1.299	−22.09	−23.389	1.26	−1.357	−22.081	−23.439	1.259
^{200}Po	−5.953	−19.033	−24.987	2.475	−1.286	−23.52	−24.806	1.22	−1.522	−23.513	−25.036	1.222
^{202}Po	−6.689	−20.394	−27.084	2.408	−1.274	−24.84	−26.114	1.19	−1.600	−24.764	−26.364	1.188
^{204}Po	−6.490	−21.077	−27.567	2.354	−1.265	−25.89	−27.155	1.16	−1.642	−25.861	−27.503	1.161
^{206}Po	−6.882	−21.819	−28.701	2.311	−1.257	−26.73	−27.987	1.14	−1.718	−26.647	−28.366	1.141
^{208}Po	−7.273	−21.893	−29.166	2.279					−1.939	−27.242	−29.181	1.126
^{210}Po	−7.712	−21.365	−29.078	2.313	−1.257	−26.24	−27.497	1.14	−2.187	−26.118	−28.305	1.142
^{212}Po	−4.712	−9.762	−14.475	2.966	−1.365	−13.41	−14.775	1.46	−1.467	−13.337	−14.804	1.466
^{214}Po	−4.952	−13.232	−18.184	2.765	−1.334	−16.42	−17.754	1.36	−1.058	−16.365	−17.424	1.366
^{216}Po	−6.501	−14.719	−21.220	2.588	−1.306	−19.47	−20.773	1.28	−1.010	−19.435	−20.445	1.278
^{218}Po	−7.571	−17.661	−25.232	2.427	−1.278	−22.65	−23.928	1.20	−0.961	−22.546	−23.507	1.199

TABLE II. PCM calculated half-life times $\log_{10} T_{1/2}$ for the α decay of $^{188-218}$Po isotopes using different assault frequencies ν_c and ν_q, and a comparison of decay half-lives is made with the experimental data [44] and calculated values of different theoretical formulas (CPPM, ADF, UDL, SLH, SLB, and SemFIS) [22,45–51]. The optimized value of neck length parameter ΔR is also shown in the table.

Parent	PCM (ν_c)		PCM (ν_q)								
nucleus	ΔR (fm)	$\log_{10} T_{1/2}$	ΔR (fm)	$\log_{10} T_{1/2}$	Expt.	CPPM	ADF	UDL	SLH	SLB	SemFIS
^{188}Po	1.92	−5.11	1.92	−5.09	−3.40	−3.50	−3.64	−4.42	−4.04	−3.43	−3.88
^{190}Po	1.91	−3.20	1.90	−3.21	−2.62	−2.38	−2.57	−3.22	−2.88	−2.23	−2.78
^{192}Po	1.93	−1.90	1.92	−1.90	−1.47	−1.21	−1.46	−1.98	−1.65	−0.98	−1.64
^{194}Po	1.61	−0.58	1.61	−0.57	−0.41	−0.08	−0.41	−0.80	−0.47	0.20	−0.53
^{196}Po	1.51	0.70	1.51	0.70	0.76	1.13	0.72	0.46	0.78	1.46	0.64
^{198}Po	1.36	2.14	1.36	2.08	2.26	2.53	2.02	1.90	2.21	2.90	2.00
^{200}Po	1.25	3.43	1.26	3.41	3.79	3.98	3.35	3.38	3.67	4.37	3.40
^{202}Po	1.35	5.47	1.32	5.47	5.15	5.32	4.57	4.74	5.02	5.73	4.69
^{204}Po	1.19	6.03	1.21	6.04	6.28	6.43	5.58	5.86	6.13	6.84	5.75
^{206}Po	1.20	7.17	1.30	7.71	7.15	7.28	6.33	6.70	6.99	7.70	6.55
^{208}Po	1.00	7.64	1.10	7.89	7.96	7.89	6.88	7.32	7.62	8.33	7.14
^{210}Po	1.20	7.55	1.20	7.54	7.08	6.75	5.81	6.18	6.56	7.26	6.04
^{212}Po	1.00	−6.45	1.00	−6.41	−6.52	−6.26	−6.62	−7.31	−6.42	−5.82	−6.57
^{214}Po	0.50	−3.41	0.50	−3.38	−3.80	−3.28	−3.68	−4.10	−3.28	−2.67	−3.65
^{216}Po	0.70	−0.35	0.70	−0.34	−0.82	−0.21	−0.72	−0.87	−0.13	0.49	−0.65
^{218}Po	0.90	3.76	0.90	3.74	2.28	3.03	2.31	2.45	3.10	3.76	2.47

the penetration probability with respect to neutron number of the daughter nucleus, N_2. The penetration probability P decreases with respect to increase in neutron number and shows behavior similar to what we observed in the case of P_0. It may be noted that the penetration probability P depends on the Q value of the decay channel [36]. We have plotted

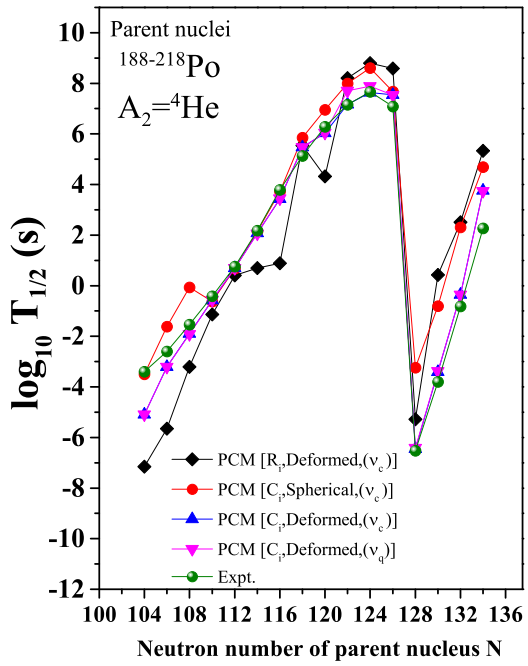

FIG. 6. PCM calculated decay half-lives using quantum assault frequency ν_q and classical assault frequency ν_c as a function of neutron number of the parent nucleus for spherical and deformed choices of the decaying fragments. The calculated decay half-lives are compared with the experimental data [44].

the Q value of the decay channel as a function of neutron number of the daughter nucleus, N_2, in Fig. 4(b). The trend of barrier penetrability P is similar to that of the Q value: both decrease till $N = 126$ and get maximum value for the case of $N_2 = 126$. Hence, the penetrability and Q value are also influenced by the shell effects. Further, the classical assault frequency ν_c and quantum assault frequency ν_q are also calculated and plotted as functions of neutron number N of the parent nucleus in Fig. 5. One can note that the assault frequencies (ν_c and ν_q) start diminishing as one approaches $N = 126$. Such variation in ν_c is basically due to the influence of the decay energy (Q value) which is shared among the two decaying fragments. Further, the global quantum number [39] plays an important role in the case of ν_q, due to which the assault frequency starts decreasing till $N = 126$. It is concluded that the assault frequency is also influenced by the shell effects of the parent nucleus. Hence, P_0, P, and ν play key roles in the α decay process, and many other theoretical approaches such as SAM and GLDM [42,43] also explore the importance of these factors for polonium isotopes. The PCM calculated P_0, P, and ν are compared with these factors in Table I. It may be noted that the PCM calculated assault frequency υ and $\log_{10} P_0 P$ value compare nicely with the literature, and few-order difference is seen for the calculated P_0 and P values. PCM is based on collective clusterization, which treats all the decay processes (such as light particle, α particle, cluster, intermediate/heavy mass fragment, and fission decay) on parallel footing. Since the PCM deals with collective clusterization approach, the relative preformation probabilities of all minimized binary fragments are calculated by solving the Schrödinger equation in the mass asymmetry coordinate η. The penetration probability is calculated in a three-step process following the excitation model of Greiner *et al.* [62]. However, In GLDM and SAM, the penetration probability P is calculated in a single-step process and the

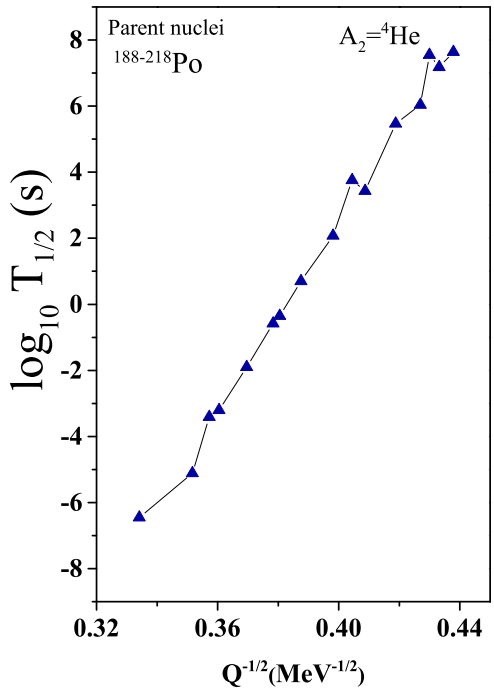

FIG. 7. The calculated $\log_{10} T_{1/2}$ as a function of $Q^{-1/2}$ for the verification of the G-N law.

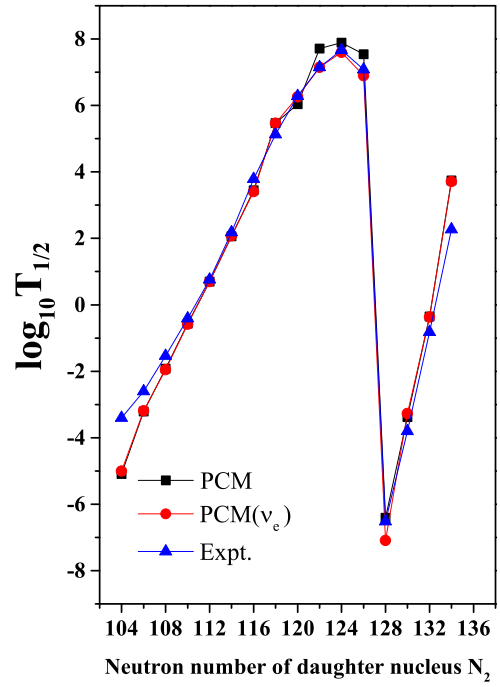

FIG. 9. The calculated decay half-lives of Po isotopes using effective assault frequency parameter (ν_e) and their comparison with previous calculations [PCM (ν_q)] and the experimental data [44].

P_0 values are given using the experimental half-lives and the empirical relation.

After studying the behavior of P_0, P and ν, the α decay half-lives are calculated using two choices of assault frequencies ν_c and ν_q and results are reported in Table II. The calculated results are compared with the available experimental data [44] and other theoretical models such as CPPM, ADF, UDL, SLH, SLB, and SemFIS [22,45–51]. It can be observed from the table that the calculated decay half-lives are in good agreement with the experimental and the theoretical data. The PCM calculated values seem independent of the assault frequencies, except for the lightest and heaviest isotopes of Po chosen for the analysis.

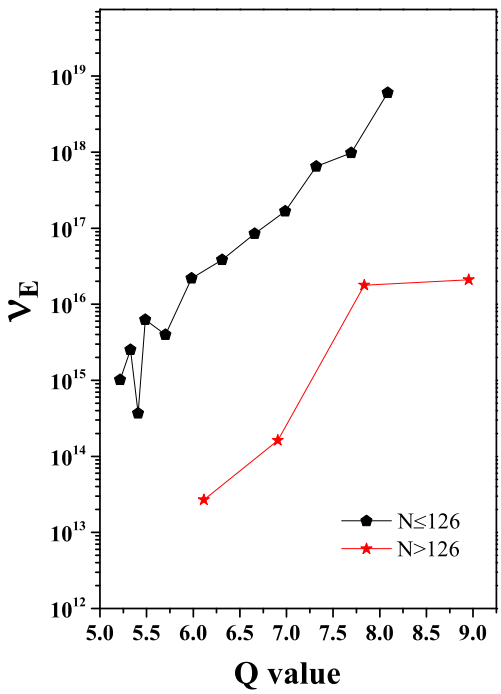

FIG. 8. The calculated effective assault frequency as a function of Q value for $N \leqslant 126$ and $N > 126$.

The calculated half-lives are plotted as a function of neutron number of the parent nucleus (N) in Fig. 6 for ν_c and ν_q using spherical and deformed choices of the decaying fragments, and comparison is made with the experimental data. It can be observed that the decay half-lives increase with increase in neutron number N of the parent nucleus, and their magnitudes are maximum at $N = 126$. This result is in agreement with the results obtained for P_0, P, and ν. The deformed choice of the decaying fragments gives better results than the spherical choice. Additionally, the half-lives calculated using C_i give better results than those using R_i. It may be concluded from the above analysis that the decay half-lives and other factors (P_0, P, and ν) strongly depend on the shell closure effects, Q value of the decay channel, and associated deformation effects. The Q value dependency on the decay half-lives can be visualized using a Geigger-Nuttal plot, where linear variation is observed between decay half-lives and $Q^{-1/2}$. After the analysis of decay half-lives, verification of the Geigger-Nuttal (G-N) plot is done by plotting $\log_{10} T_{1/2}$ vs $Q^{-1/2}$ in Fig. 7. It is observed that $\log_{10} T_{1/2}$ varies almost linearly with increase in the value of $Q^{-1/2}$, with slope 141.437 and intercept −54.04. Hence, the calculated $T_{1/2}$ are in agreement with the G-N law, which means that the decay half-lives are strongly influenced by the Q value of the exit channel.

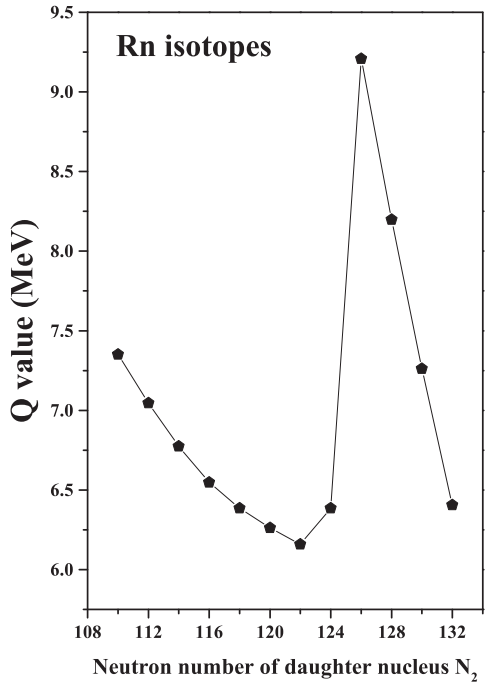

FIG. 10. The calculated Q value for Rn isotopes as a function of neutron number of the daughter nucleus.

B. Study of the effective assault frequency of polonium isotopes

In the previous section, behavior of penetration probability P, preformation probability P_0, and the assault frequency ν is studied with respect to the neutron number of the daughter fragment (N_2) or that of the parent nucleus (N). It is concluded that all of the three parameters play crucial roles in the stability analysis of the radioactive nucleus. The stability further depends on the shell effects and the Q value of the decay channel. In the past [40,41] different preformation parameter or assault frequency parameter values were introduced which depend on the Q value, isospin, and the charge number of the daughter nucleus accompanying the α particle. Additionally, some parameters are given which contain both assault frequency and preformation factor. Such a parameter is known as the modified assault frequency or effective assault frequency (ν_e). Following this work, the product of the quantum mechanical assault frequency (ν_q) and the preformation probability is plotted as a function of Q value for $N \leqslant 126$ and $N > 126$ and shown in Fig. 8. It can be observed from the figure that the effective assault frequency increases with increase in the Q value. Using this plot a second-order polynomial is obtained which is basically assault frequency parameter as a function of Q value as given by

$$\log_{10} \nu_e = AQ^2 + BQ + C \tag{17}$$

where $A = -0.063\,15$, $B = 2.100\,74$, and $C = 5.767\,66$ for $N \leqslant 126$ and $A = -0.537\,02$, $B = 8.9285$, and $C = -19.911\,52$ for $N > 126$. The validity of these parameters is analyzed by calculating the decay half-lives of the polonium isotopes using Eq. (17). The ν_e calculated decay half-lives are compared with the calculations performed in Sec. III A and the experimental data and shown in Fig. 9. Here in the plot PCM (ν_q) denotes the calculations which are performed in Sec. III A and PCM (ν_e) is the calculations performed using the frequency parameter [Eq. (17)]. It can be observed

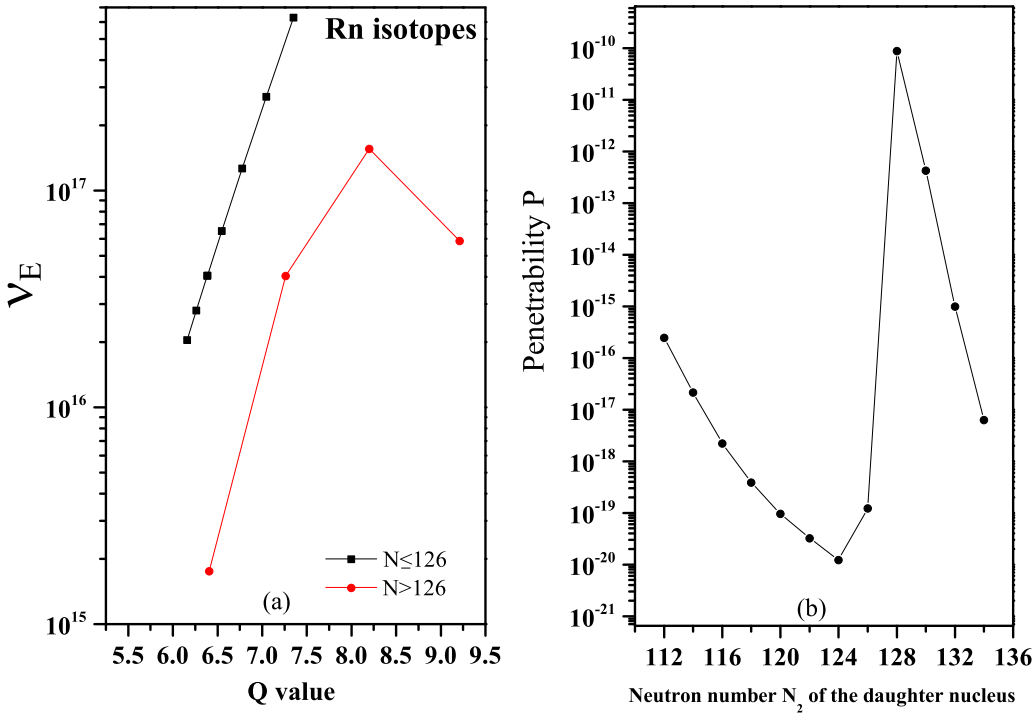

FIG. 11. The calculated (a) effective assault frequency (ν_e) and (b) barrier penetrability P as a function of neutron number of the daughter nucleus, N_2.

TABLE III. PCM calculated half-life times $T_{1/2}$ for the α decay of $^{198–220}$Rn isotopes using effective assault frequencies ν_e; a comparison is made with experimental data [44]. The optimized value of neck length parameter ΔR and Q value are also shown in the table.

Parent	Q value	PCM (ν_E)		Expt.
nucleus	(MeV)	ΔR (fm)	$\log_{10} T_{1/2}$	$\log_{10} T_{1/2}$
^{198}Rn	7.351	1.92	−2.35	−1.19
^{200}Rn	7.045	1.85	0.07	0.04
^{202}Rn	6.775	1.92	0.391	1.04
^{204}Rn	6.547	1.90	1.437	2.00
^{206}Rn	6.385	1.92	2.89	2.74
^{208}Rn	6.262	1.93	2.90	3.38
^{210}Rn	6.159	1.92	3.44	3.95
^{212}Rn	6.386	1.90	2.15	3.16
^{214}Rn	9.209	1.35	−6.87	−6.57
^{216}Rn	8.198	1.30	−4.98	−4.35
^{218}Rn	7.262	1.35	−1.76	−1.46
^{220}Rn	6.405	1.00	1.79	1.75

from the figure that PCM (ν_e) calculated decay half-lives are in good agreement with the PCM (ν_q) results and the experimental data. Hence one may use Eq. (17) to calculate the half-lives, where the Q value lies in the range 5–10 MeV.

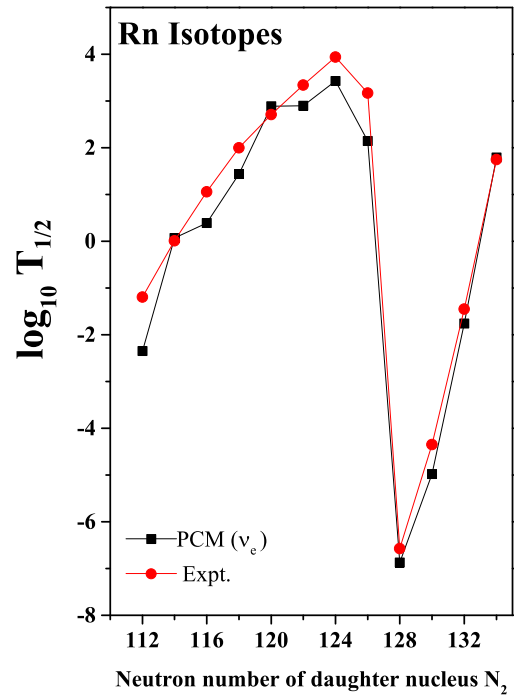

FIG. 12. The calculated decay half-lives using the effective assault frequency (ν_e) and barrier penetrability, and their comparison with the available experimental data.

C. Verification of effective assault frequency parameter

In the previous section effective assault frequency parameter ν_e is obtained, and half-lives calculated using this parameter are in agreement with the experimental data. In this section, α decay half-lives of $^{198–220}$Rn isotopes are calculated using effective assault frequency ν_e discussed in the last section. First, the Q value is calculated for the α decay channel from Rn ($Z = 84$) isotopes. The calculated Q value is plotted as function of neutron number of the daughter nucleus N_2, in Fig. 10. It can be observed from the figure that the Q value is minimum for $N = 126$ and maximum for $N = 128$, hence the importance of shell effects is evident for Rn isotopes. As a next step, the effective assault frequency ν_e and the penetration probability P are calculated and plotted as a function of neutron number N_2 and shown in Figs. 11(a) and 11(b). The ν_e parameter varies linearly for $N \leqslant 126$ and has parabolic variation in the case of $N < 126$. The calculated penetration probability is minimum near $N = 126$. After calculation of ν_e and penetration probability P, decay half-lives are calculated and compared with the experimental data as shown in Table III. The calculated neck parameter and the Q value are also shown in the table. The calculated half-lives are in good agreement with the experimental data [44]. The calculated decay half-lives of Rn isotopes are plotted as a function of neutron number of the parent nucleus, N, in Fig. 12. The decay half-lives are more for $N = 126$. Hence the importance of shell closure effects is also observed in the case of Rn isotopes. The effective assault frequency parameter ν_e successfully addressed the experimental half-lives and the shell closure effects. Hence, we may incorporate this parameter to find the α decay half-lives of radioactive nuclei.

IV. SUMMARY

Summarizing, the α decay analysis of $^{188–218}$Po isotopes is carried out using the preformed cluster model (PCM). The barrier characteristics of the α decay channel are studied with and without the inclusion of the surface diffuseness parameter. The fragmentation structure of ^{188}Po, ^{202}Po, and ^{218}Po isotopes is explored, where the α particle is found to be the most probable decay fragment for the chosen set of Po isotopes. The preformation probability, barrier penetration probability, and assault frequency (classical and quantum) are calculated and influence of neutron shell closure of the parent nucleus is explored. The PCM calculated P_0, P, and ν are compared with the different theoretical approaches. The classical mode of the assault frequency (ν_c) depends on the Q value of the decay channel and the quantum mechanical mode (ν_q) depends on the global quantum number. The decay half-lives of α emission are calculated using both choices of assault frequency and a comparison is made with the results of CPPM, ADF, UDL, SLH, SLB, an SemFIS and with the available experimental data. The deformed (β_2) choice of the decaying fragments gives better agreement with the experimental data as compared to the spherical choice. The calculated α decay half-life is found to be maximum near $N = 126$. The verification of G-N law is done using the calculated decay half-lives, and their dependency on the Q value of the decay channel is explored. The effective assault frequency parameter ν_e is obtained using P_0 and the quantum assault frequency (ν_q). The

α decay half-lives are calculated using ν_e and are found to be in good agreement with the experimental data for Po and Rn isotopes. It will be of further interest to calculate the effective assault frequency ν_e parameter for other probable ground state decay mechanisms (such as CR, HPR, SF, etc.) for heavy and superheavy mass regions.

ACKNOWLEDGMENTS

Financial support from the Department of Science and Technology (DST), New Delhi, India in the form of a research project grant (File No. CRG/2021/001144) is gratefully acknowledged.

[1] A. Allisy, Radiat. Prot. Dosim. **68**, 3 (1996).
[2] E. Hourani *et al.*, Ann. Phys. (Paris) **14**, 311 (1989).
[3] D. N. Poenaru *et al.*, Europhys. Lett. **118**, 22001 (2017).
[4] D. N. Poenaru and R. A. Gherghescu, Phys. Rev. C **94**, 014309 (2016).
[5] Y. Z. Wang, S. J. Wang, Z. Y. Hou, and J. Z. Gu, Phys. Rev. C **92**, 064301 (2015).
[6] A. C. Wahl, At. Data Nucl. Data Tables **39**, 1 (1988).
[7] A. Parkhomenko and A. Sobiczewski, Acta Phys. Pol. B **36**, 1363 (2005).
[8] Yu. Oganessian, Radiochim. Acta **99**, 429 (2011).
[9] J. H. Hamilton *et al.*, Annu. Rev. Nucl. Part. Sci. **63**, 383 (2013).
[10] D. N. Poenaru *et al.*, J. Phys. G: Nucl. Part. Phys. **32**, 1223 (2006).
[11] A. Staszczak, A. Baran, and W. Nazarewicz, Phys. Rev. C **87**, 024320 (2013).
[12] D. N. Poenaru and R. A. Gherghescu, J. Phys. G: Nucl. Part. Phys. **41**, 125104 (2014).
[13] D. N. Poenaru *et al.*, Eur. Phys. J. A **54**, 14 (2018).
[14] L. Capponi *et al.*, Phys. Rev. C **94**, 024314 (2016).
[15] D. N. Poenaru and W. Greiner, *Handbook of Nuclear Properties* (Clarendon, Oxford, 1996).
[16] D. N. Poenaru, *Nuclear Decay Modes* (Institute of Physics, Bristol, 1996).
[17] D. T. Akrawy *et al.*, Nucl. Phys. A **1021**, 122419 (2022).
[18] H. B. Yang *et al.*, Phys. Rev. C **105**, L051302 (2022).
[19] A. N. Bezbakh, G. G. Adamian, and N. V. Antonenko, Phys. Rev. C **105**, 054305 (2022).
[20] K. P. Santhosh, T. A. Jose, and N. K. Deepak, Phys. Rev. C **105**, 054605 (2022).
[21] D. N. Poenaru *et al.*, Comput. Phys. Commun. **25**, 297 (1982).
[22] D. T. Akrawy and D. N. Poenaru, J. Phys. G: Nucl. Part. Phys. **44**, 105105 (2017).
[23] D. N. Poenaru and R. A. Gherghescu, Phys. Rev. C **97**, 044621 (2018).
[24] K. Varga, R. G. Lovas, and R. J. Liotta, Phys. Rev. Lett. **69**, 37 (1992).
[25] I. Ahmad *et al.*, Phys. Rev. C **8**, 737 (1973).
[26] D. N. Poenaru and R. A. Gherghescu, Europhys. Lett. **124**, 52001 (2018).
[27] G. Royer and R. A. Gherghescu, Nucl. Phys. A **699**, 479 (2002).
[28] N.-N. Ma *et al.*, Chin. Phys. C **45**, 024105 (2021).
[29] J.-G. Deng, J. C. Zhao, P. C. Chu, and X. H. Li, Phys. Rev. C **97**, 044322 (2018).
[30] D. Bai *et al.*, Chin. Phys. C **42**, 124102 (2018).
[31] D. N. Poenaru *et al.*, Phys. Rev. C **32**, 572 (1985).
[32] D. N. Poenaru *et al.*, At. Data Nucl. Data Tables **34**, 423 (1986).
[33] A. Kaur, N. Sharma, and M. K. Sharma, Phys. Rev. C **103**, 034618 (2021).
[34] N. Sharma, A. Kaur, and M. K. Sharma, Phys. Rev. C **102**, 064603 (2020).
[35] S. S. Malik and R. K. Gupta, Phys. Rev. C **39**, 1992 (1989).
[36] K. Sharma, G. Sawhney, and M. K. Sharma, Phys. Rev. C **96**, 054307 (2017).
[37] K. Sharma *et al.*, Nucl. Phys. A **972**, 1 (2018).
[38] R. K. Gupta and W. Greiner, Int. J. Mod. Phys. E **03**, 335 (1994).
[39] H. F. Zhang, G. Royer, and J.Q. Li, Phys. Rev. C **84**, 027303 (2011).
[40] V. Yu. Denisov and A. Khudenko, At. Data Nucl. Data Tables **95**, 815 (2009).
[41] V. Yu. Denisov and A. A. Khudenko, Phys. Rev. C **80**, 034603 (2009).
[42] M. Ismail *et al.*, J. Phys. G: Nucl. Part. Phys. **47**, 055105 (2020).
[43] H. F. Zhang and G. Royer, Phys. Rev. C **77**, 054318 (2008).
[44] S. B. Duarte *et al.*, At. Data Nucl. Data Tables **80**, 235 (2002).
[45] D. N. Poenaru, E. Hourany, W. Greiner, in *Nuclear Decay Modes*, edited by D. N. Poenaru (Institute of Physics, Bristol, 1996), pp. 204–236, Chap. 4.
[46] D. N. Poenaru, I. H. Plonski, and W. Greiner, Phys. Rev. C **74**, 014312 (2006).
[47] C. Qi, F. R. Xu, R. J. Liotta, and R. Wyss, Phys. Rev. Lett. **103**, 072501 (2009).
[48] C. Qi, F. R. Xu, R. J. Liotta, R. Wyss, M. Y. Zhang, C. Asawatangtrakuldee, and D. Hu, Phys. Rev. C **80**, 044326 (2009).
[49] B. A. Brown, Phys. Rev. C **46**, 811 (1992).
[50] M. Horoi, J. Phys. G: Nucl. Part. Phys. **30**, 945 (2004).
[51] S. S. Hosseini *et al.*, Nucl. Phys. A **970**, 259 (2018).
[52] J. Maruhn and W. Greiner, Phys. Rev. Lett. **32**, 548 (1974).
[53] R. K. Gupta, W. Scheid, and W. Greiner, Phys. Rev. Lett. **35**, 353 (1975).
[54] R. K. Gupta, A. Sandulescu, and W. Greiner, Phys. Lett. B **67**, 257 (1977)
[55] K. Wildermuth and Y. C. Tang, *A Unified Theory of the Nucleus* (Academic, New York, 1977).
[56] P. Mohr, Phys. Rev. C **61**, 045802 (2000)
[57] B. Buck, A. C. Merchant, and S. M. Perez, Phys. Rev. C **51**, 559 (1995).
[58] M. Wang *et al.*, Chin. Phys. C **36**, 1603 (2012).
[59] P. Möller, J. R. Nix, W. D. Myers, and W. J. Swiatecki, At. Data Nucl. Data Tables **59**, 185 (1995).
[60] J. Blocki, W. J. Swiatecki, and C. F. Tsang, Ann. Phys. (NY) **105**, 427 (1977).
[61] R. Kumar and M. K. Sharma, Phys. Rev. C **85**, 054612 (2012).
[62] M. Greiner and W. Scheid, J. Phys. G **12**, L229 (1986).
[63] G. Süssmann, Z. Phys. A **274**, 145 (1975).
[64] S. Dahmardeh, A. Alavi, and V. Dehghani, Nucl. Phys. A **963**, 68 (2017).
[65] G. G. Adamian, Phys. Rev. C **90**, 034322 (2014).
[66] R. K. Gupta, S. Singh, R. K. Puri, and A. Sandulescu, J. Phys. G: Nucl. Part. Phys. **18**, 1533 (1992).